

Article

# Self-Immobilizing Biocatalysts Maximize Space–Time Yields in Flow Reactors

Theo Peschke , Patrick Bitterwolf, Silla Hansen, Jannis Gasmi, Kersten S. Rabe  and Christof M. Niemeyer \* 

Karlsruhe Institute for Technology (KIT), Institute for Biological Interfaces (IBG 1), Hermann-von-Helmholtz-Platz 1, D-76344 Eggenstein-Leopoldshafen, Germany; theo.peschke@kit.edu (T.P.); patrick.bitterwolf@kit.edu (P.B.); silla.hansen@kit.edu (S.H.); jannisgasmi@gmx.de (J.G.); Kersten.rabe@kit.edu (K.S.R.)

\* Correspondence: niemeyer@kit.edu; Tel.: + 497-216-082-3000

Received: 17 January 2019; Accepted: 5 February 2019; Published: 8 February 2019



**Abstract:** Maximizing space–time yields (STY) of biocatalytic flow processes is essential for the establishment of a circular biobased economy. We present a comparative study in which different biocatalytic flow reactor concepts were tested with the same enzyme, the (*R*)-selective alcohol dehydrogenase from *Lactobacillus brevis* (LbADH), that was used for stereoselective reduction of 5-nitrononane-2,8-dione. The LbADH contained a genetically encoded streptavidin (STV)-binding peptide to enable self-immobilization on STV-coated surfaces. The purified enzyme was immobilized by physisorption or chemisorption as monolayers on the flow channel walls, on magnetic microbeads in a packed-bed format, or as self-assembled all-enzyme hydrogels. Moreover, a multilayer biofilm with cytosolic-expressed LbADH served as a whole-cell biocatalyst. To enable cross-platform comparison, STY values were determined for the various reactor modules. While mono- and multilayer coatings of the reactor surface led to  $STY < 10$ , higher productivity was achieved with packed-bed reactors ( $STY \approx 100$ ) and the densely packed hydrogels ( $STY > 450$ ). The latter modules could be operated for prolonged times (>6 days). Given that our approach should be transferable to other enzymes, we anticipate that compartmentalized microfluidic reaction modules equipped with self-immobilizing biocatalysts would be of great utility for numerous biocatalytic and even chemo-enzymatic cascade reactions under continuous flow conditions.

**Keywords:** enzymes; flow biocatalysis; immobilization techniques; stereoselective reactions; biomaterials; micro reactors

## 1. Introduction

Enzymes are highly efficient and specific catalysts, continuously changed by nature through evolution since the beginning of life. Their industrial implementation is expected to have an enormous impact on the emergence of a biobased circular economy or “bioeconomy” [1,2]. To establish the efficient use of renewable biomass as an alternative to petrochemical synthesis for sustainable production processes in the future, the barrier of economic viability of enzyme processes has to be overcome. While recent progress in the field of industrial biocatalysis for the production of pharmaceutical drugs, such as Montelukast (Singulair® by MSD) [3], Atorvastatin (Sortis®, Atorvalan®, or Lipitor® by Pfizer) [4], Ipatasertib (Roche) [5], and Sitagliptin (MSD) [6], clearly indicates the feasibility of this approach, further improvement of such processes will crucially depend on the availability of flexible technical production platforms. In view of these developments, miniaturized flow reactors that enable enzymatic multistep reactions are currently attracting much attention [7–13]. Facilitating the production of value-added molecules by conventional organic synthesis reaction

cascades can be realized by the precise arrangement of spatially separated sequential transformations within individual reaction vessels that are fluidically coupled with each other. In classical synthetic organic chemistry, this approach is known as “flow chemistry”. It takes advantage of a high degree of control over temperature profiles and diffusion-based mixing along with machine-assisted automation [14] and has recently yielded impressive synthesis campaigns for small molecules [15–17]. In contrast to flow chemistry, and despite the high attractiveness of enzymatic transformations, continuous “flow biocatalysis” is still in its infancy [13,18–26].

One of the major challenges that hampers the broad application of biocatalytic processes in flow systems stems from a limited number of appropriate methods for the immobilization of delicate enzymes, which are usually more demanding than conventional organometallic catalysts [27]. Common approaches for enzyme immobilization inside microstructured flow channels include non-specific physisorption and chemical cross-linking, as well as more sophisticated and often more efficient methods that are based on directional bioorthogonal one-point immobilization strategies, mediated by genetically encoded immobilization tags [28]. While these methods have proven their applicability [13,20,21,29–31], another important problem stems from the limitation on the amount of immobilized biocatalyst which is determined by the effective surface area. This issue has, for example, been addressed by the use of pseudo-3D interfacial layers comprising synthetic polymers or micro-/nanoparticles that increase the number of binding sites and, thus, the loading capacity for enzymes [32–34] with a concomitant maximization of the reactor space–time yields. These approaches are not limited to purified enzymes as whole-cell biocatalysts can also be applied to build up 3-dimensional production systems, as exemplified by productive biofilms for continuous production processes of fine chemicals [35]. However, comparative studies utilizing the same enzyme, either in a purified formulation or else expressed as whole-cell biocatalysts, in different flow reactor setups are still lacking.

To further contribute to the systematic development of flow biocatalysis, we describe here a comprehensive comparison of five different biocatalytic flow-reactor concepts that are based on the same enzyme, the industrial relevant and intensively studied (*R*)-selective alcohol dehydrogenase (ADH, EC 1.1.1.2) from *Lactobacillus brevis* ATCC 14869 (LbADH) (Taxonomy ID: 649758) [36]. A typical flow biocatalytic work station used for this study consists of syringe pumps connected to a chip micro reactor harboring the biocatalyst and an automated outflow collector for subsequent sample analysis (Figure 1a). Depending on the requirements of the individual biocatalyst, meander-shaped flow channels were employed for physisorbed or chemically immobilized enzymes, as well as productive biofilms (Figure 1b), whereas linear flow channels were used for packed-bed reactors harboring enzyme-functionalized magnetic particles (Figure 1c) or self-assembling all-enzyme hydrogels (Figure 1d). To enable cross-platform assessment and comparison of the productivity of the various flow biocatalyst modules, differences in reactor volume and flow rates were compensated for by the determination of STY. To account for variations in reactor volume due to variable quantities of biomass and carrier/adsorbed materials, space–time yields were calculated on the basis of the reactor geometry.

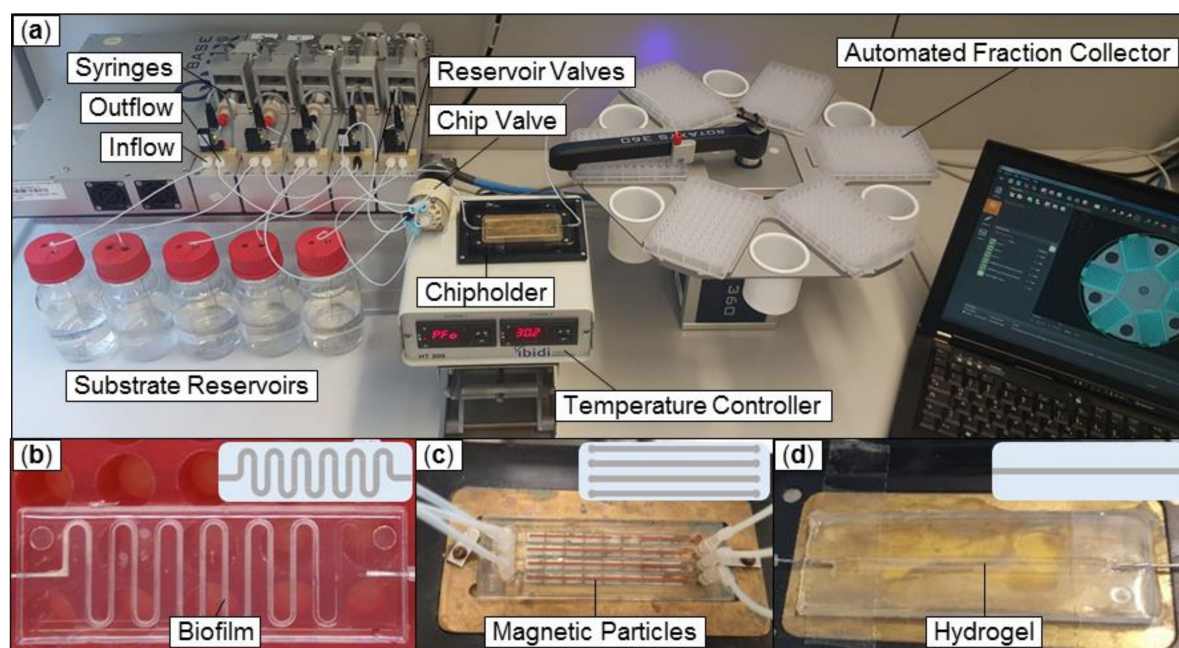


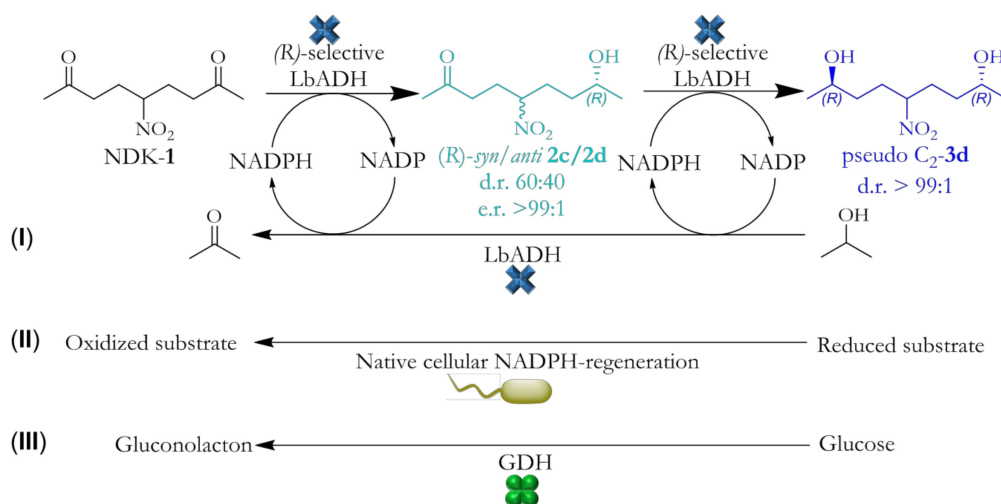
**Figure 1.** Setup for continuous flow biocatalysis using microfluidic chip reactors. (a) Overview of the microfluidic system with photo and scheme of (b) polydimethylsiloxane (PDMS) chip with meandering flow path containing a productive *Escherichia coli* biofilm. (c) polymethylmethacrylate (PMMA) chip with permanent magnets arranged beneath the flow channel holding enzyme-functionalized magnetic particles (brown). (d) PDMS chip with pure all-enzyme hydrogel in a straight flow path.

## 2. Results and Discussion

To explore and validate the utility of the different reactor modules for immobilization of the (*R*)-selective alcohol dehydrogenase LbADH, we used the prochiral  $C_5$ -symmetrical 5-nitrononane-2,8-dione (NDK) **1** (Scheme 1), which can be reduced, depending on the ADH selectivity, either on one or both of the two carbonyl functions to create the hydroxyketones **2** or diols **3**, respectively [37]. Since all stereoisomeric products can be readily analyzed by chiral HPLC, the two-step enantioselective reduction of the prochiral NDK **1** is ideally suited to characterizing the biocatalytic activity of a given flow biocatalysis reactor. To enable a simple downstream process, the LbADH sequence was N-terminally extended by the 39 amino acid streptavidin-binding peptide (SBP) tag [38] that binds with high affinity ( $K_D = 2.5$  nM) to the protein streptavidin (STV) [39], enabling a simple one-step purification. The LbADH-SBP was overexpressed in *Escherichia coli* and purified to homogeneity using STV-affinity chromatography. Details on the reaction kinetics and stereoselectivity for the reduction of the NDK **1** substrate of the LbADH-SBP were recently described [30]. As shown in Scheme 1, LbADH-SBP converts NDK **1** in a highly stereoselective manner to (*R*)-syn/anti-hydroxyketones **2c/d** (e.r. > 99:1; d.r. ~ 60:40) and then further to (*R,R*)-configured pseudo  $C_2$ -diol **3d** (d.r. 99:1).

To cope with the high demand for the expensive cofactor, nicotinamide adenine dinucleotide phosphate (NADPH), three different strategies were used in this study (Scheme 1). The simplest approach used the ability of LbADH to regenerate its own cosubstrate through the oxidation of 2-propanol to acetone [36] (Scheme 1, I). However, the LbADH productivity was found to be lower due to additional oxidation of 2-propanol to acetone [30]. Therefore, employment of an additional enzyme for the regeneration of the cofactor was found to be more effective. In the case of whole-cell biocatalysis with the cytosolically-expressed LbADH, the native cellular metabolisms of the host were utilized for NADPH-regeneration (Scheme 1, II). As a third option, the in-situ NADPH-regeneration utilizing “helper”-enzymes (Scheme 1, III), such as the glucose 1-dehydrogenase GDH (EC 1.1.1.47) from *Bacillus subtilis subsp. natto* (Taxonomy ID: 86029), was explored. In comparison to other NADPH-regeneration

enzymes, such as formate-/lactate-decarboxylases, GDH does not produce CO<sub>2</sub>-gas bubbles, which are detrimental for microfluidic processes.



**Scheme 1.** NDK 1 reduction employing different methods for NADPH-cofactor regeneration. Note that for simplicity, only (R)-selective reaction products are shown; for the structure of the corresponding (S)-selective reaction products, i.e., the syn/anti hydroxyketones **2a/2b** and (S,S) pseudo C<sub>2</sub>-diol **3c** or meso syn/anti diols **3a/3b**, see reference [37]. The NADPH cofactor can be regenerated by (I) the oxidation of isopropanol to acetone; (II) in the case of whole-cell biocatalysis, the host's native cellular metabolisms; or (III) an additional "helper"-enzyme such as glucose dehydrogenase (GDH).

As an initial experiment, we tested physisorption of the enzyme of choice to the reactor surface, because this method was widely applied and simple. To this end, a recently described polydimethylsiloxane (PDMS) chip design [40] with a meandering flow path of 150  $\mu$ L total internal volume was incubated with 10  $\mu$ M LbADH–SBP enzyme solution overnight at 4  $^{\circ}$ C. The unbound enzymes were stripped from the reactor wall by continuous perfusion with a PBS buffer. The temperature was then increased to 30  $^{\circ}$ C and the reactor perfused at a flowrate of 2  $\mu$ L/min with a substrate solution containing NDK 1, NADP<sup>+</sup> cofactor, and 5% (v/v) 2-propanol for cofactor-regeneration (Scheme 1, I). In order to analyze the NDK-reduction activity of the reactor, samples from the outflow were analyzed by quantitative chiral HPLC-analysis. We found that the physisorbed LbADH–SBP in the reactor module was not sufficient to convert NDK 1 (Figure 2a). We attributed this result to the inefficient immobilization strategy in terms of low binding efficiency and possible concurrent deactivation of the enzyme. To validate this hypothesis and to increase the effectiveness of enzyme immobilization on the reactor walls, we employed a procedure for covalent immobilization by initially coating the PDMS chip with (3-aminopropyl) triethoxysilane (APTES). The surface-bound amino groups were utilized for covalent immobilization of the LbADH–SBP surface using glutaraldehyde crosslinking. Indeed, the so-prepared chip showed 15% NDK conversion to 14% (R)-syn/anti-hydroketone **2c/d** with only small amounts (1%) of diol **3d** produced (Figure 2a).

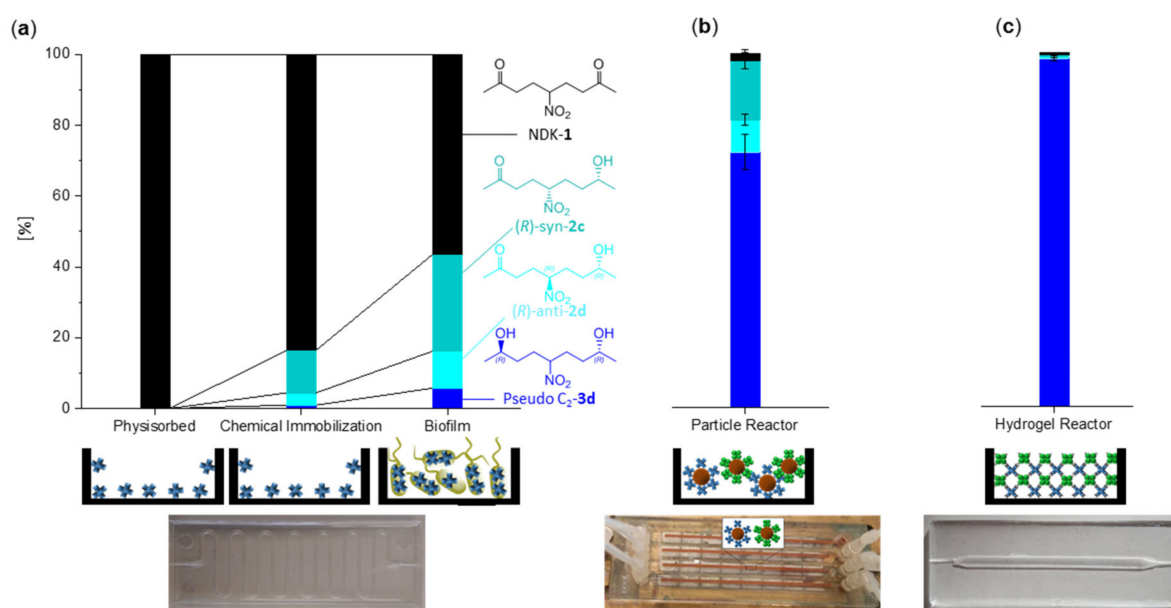


**Figure 2.** Flow biocatalytic conversion of NDK **1** to (*R*)-syn/anti-hydroketone **2c/d** and diol **3d**. The bar graphs show the product distribution obtained from the various different reactor modules, i.e., the meander channel (a) with physisorbed or chemically immobilized pure enzyme or whole-cell biofilm intracellularly expressing the LbADH–SBP, (b) the packed-bed reactor with LbADH–SBP and GDH–SBP immobilized on individual magnetic particles and (c) the all-enzyme LbADH–SC/GDH–ST hydrogel filled reactor module. All modules were perfused with a substrate solution containing 10 mM NDK **1**. Product distributions were determined by quantitative HPLC analysis. Note that the stereoselectivity of all reactor modules was determined exclusively by the incorporated LbADH.

In order to relate the results with the purified enzyme in this reactor geometry to a whole-cell biocatalysis approach, we used a previously developed whole-cell system that would express the enzyme cytosolically [41]. Here, we used the meander channel to grow 3-dimensional biofilms that would be capable of utilizing the native NADP(H) regeneration of *E. coli* (Scheme 1, II). Growth of the biofilm was achieved by inoculation and initial perfusion of the chip for 24 h before protein expression was induced by supplementation of the media with IPTG. After another 24 h, NDK **1** was supplemented to the reaction media to facilitate continuous biotransformation. Productivity of the biofilm was determined by HPLC analysis. The analysis of the outflow from this reactor module showed 43% NDK conversion to form 37% (*R*)-syn/anti-hydroketone **2c/d** with up to 6% of the wanted diol **3d** product. This represents a significant improvement of the reactor productivity.

To evaluate the extent to which more complex immobilization processes can lead to improved productivity in flow biocatalysis, we then investigated a recently described modular packed-bed reactor setup that contained streptavidin (STV)-functionalized magnetic microparticles to enable selective one-point immobilization of LbADH–SBP from crude cell lysates [30]. To further increase the productivity of the reactor we co-immobilized SBP-tagged GDH as a helper enzyme (Scheme 1, III). As indicated in Figure 2b, the resulting biocatalytic reactor modules showed 98% NDK conversion predominantly producing the desired diol **3d** product (70%) along with 28% of the (*R*)-syn/anti-hydroketones **2c/d**, when perfused with NDK **1** at a flowrate of 1  $\mu$ L/min. Very importantly, this setup enables long operating times of more than five days, thereby indicating stable enzyme immobilization and general robustness of the reactor [30]. Despite these advantages, the available volume of the reactor module is far from being optimally used: Taking into account an enzyme binding capacity of  $\sim 10$   $\mu$ g/mg particles [30], the maximal enzyme capacity of the module can only be 1% (w/w) enzyme per carrier material. This assessment shows that 99% of the available reactor space is filled with non-catalytic materials.

Since the incorporation of any type of carrier materials inevitably reduces the amount of biocatalyst in the reactors, it is evident that the application of carrier-free immobilization strategies could further increase the productivity of flow reactors. To make better use of the space reserves, we recently developed self-assembling all-enzyme hydrogels that were produced by genetically encoded cross-linking of pure enzymes [23]. To this end, the enzymes LbADH and GDH were employed and genetically fused with either the SpyTag (ST) or the SpyCatcher (SC) [42]. The ST/SC system enables the rapid cross-linking of the two tetravalent protein building blocks through the formation of covalent isopeptide bonds under physiological conditions, resulting in the formation of a pure LbADH-SC/GDH-ST hydrogel. Here, we used this novel biocatalytic material for the loading of a 150  $\mu\text{L}$  straight flow channel in a microfluidic PDMS chip to generate a hydrogel-reactor module (Figure 2c). Indeed, this bioreactor enabled the continuous production of the desired diol product **3d** in a purity of >99%, at the same flowrate of 1  $\mu\text{L}/\text{min}$  that had been applied to the packed-bed reactor (Figure 2b).

Given the outstanding productivity of all-enzyme reactor modules, we further investigated the process stability and productivity of these systems by analyzing the outflow at flowrates from 1–200  $\mu\text{L}/\text{min}$  (Figure 3a). Indeed, the concentration of the diol **3d** product in the reactor outflow decreased from >99% at a flowrate of 1  $\mu\text{L}/\text{min}$  to  $15 \pm 3\%$  at 200  $\mu\text{L}/\text{min}$ . Remarkably, the hydrogel reactor still produced substantially higher amounts of the diol **3d** even when it was operated at a flowrate 10 times that of the particle reactor. These results impressively illustrate the high robustness and catalytic activity of the hydrogel reactor module. The high initial activity of the reactor only slightly decreased when operated for a prolonged time over five days (Figure 3b). We hypothesize that the initial slight decrease of the reactor performance was caused by the outflow of unassembled all-enzyme hydrogel building blocks.

Since the industrial implementation of enzymatic flow processes is difficult when expensive cofactors (e.g., NADPH) need to be supplemented continuously [43], we also investigated the influence of the operational flow rate on the product distribution for reactor modules that contained all-enzyme hydrogels in which NADPH was entrapped during the polymerization step. To this end, the modules were loaded with all-enzyme hydrogels bearing 1 mM co-entrapped NADP<sup>+</sup> and perfused with a reaction buffer containing only glucose and NDK. Indeed, the NDK was continuously converted for more than 30 h with only a minor decrease in reactor performance. These results show that the entrapped NADPH cofactor was effectively retained in the hydrogel matrix to enable the conversion of more than 120 reactor column volumes (Figure 3c).

For a comparison of the reactor space productivity of the various flow biocatalyst modules, we compared all of the established systems in terms of volumetric reactor productivity of the diol **3d** product by calculating the respective STY. Figure 4 shows that the various platforms revealed huge differences in STY. While the systems based on the reactor surface modification with only one layer of physisorbed or chemically immobilized enzymes resulted in an STY <1  $\text{g L}^{-1} \text{day}^{-1}$ , multilayers of catalytically active biofilms showed an STY of 4.6  $\text{g L}^{-1} \text{day}^{-1}$ . Much higher STY values of 102  $\text{g L}^{-1} \text{day}^{-1}$  could be obtained with the particle reactor. We attribute this result to the fact that the introduced particles increased the available reactor surface by approximately 50 times, thereby increasing the concomitant enzyme binding capacity. However, the effect of a better utilization of the available reactor volume was significantly increased by the use of carrier-free self-assembled all-enzyme hydrogels. In this case, the hydrogel-filled reactor modules showed an STY, 4.5 times higher, of 487  $\text{g L}^{-1} \text{day}^{-1}$ . This clearly demonstrates the advantages of carrier-free immobilization strategies to maximize the STY of biocatalytic reactors. Considering the diol **3d** productivity of the different systems per chip, this corresponds to a 73-fold increase in chip productivity of the 150  $\mu\text{L}$  hydrogel reactor ( $73 \text{ mg day}^{-1}$ ) as compared to the 10  $\mu\text{L}$  particle reactor ( $1 \text{ mg day}^{-1}$ ).

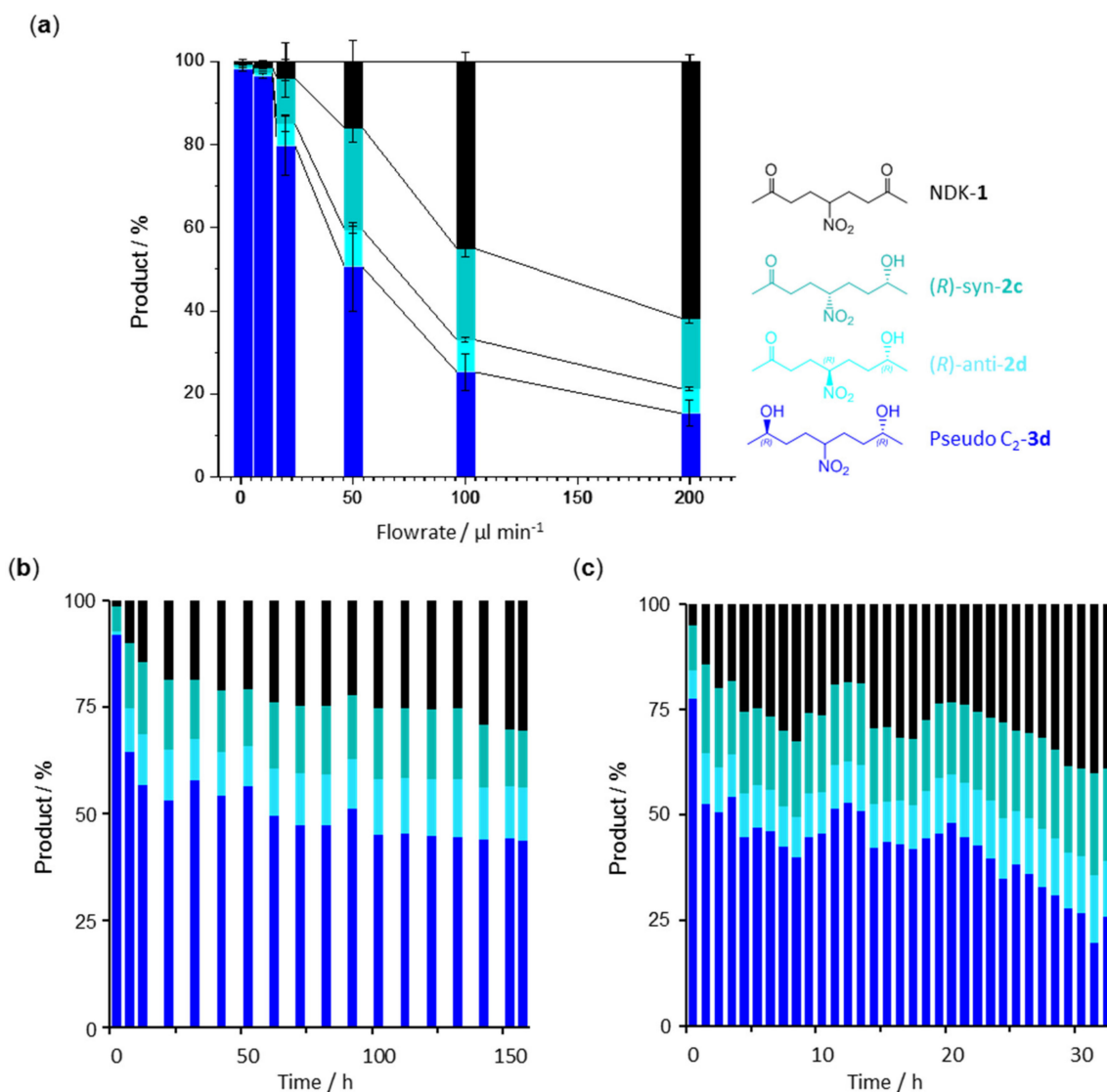


**Figure 3.** Product distributions determined in the outflow of reactor modules containing the LbADH-ST/GDH-SC hydrogel: (a) Flowrate dependency; (b) long-term time dependency with continuous NADP<sup>+</sup>-supply over >6 days (flowrate 10 µL/min); (c) time dependency with encapsulated NADP<sup>+</sup> (flowrate 10 µL/min).

In conclusion, for the first time we have provided a comparative study in which different technical platforms for flow biocatalysis are tested with the same enzyme. The results clearly showed that self-immobilizing biocatalysts, used either in a purified formulation [23,30] or as whole cell biocatalysts [41], could be advantageously applied to maximize the STY in flow-reactors. As expected, the efficient utilization of the available reactor space plays a decisive role. While simple mono- and multilayer coatings of the reactor surface lead to STY <10, these values can be considerably increased by using three-dimensional space. Specifically, with packed-bed reactors, values of 100 were achieved. With room-filling packed hydrogels, values of >450 were achieved. Even without detailed optimization of the flow and reaction conditions, continuous production for more than six days can be achieved. Hence, such biocatalytic reactors are, in principle, ready for practical applications. An important issue is that self-immobilizing biocatalysts can often be employed without extensive purification, thereby significantly reducing time and costs for process development.

A general advantage for the industrial use of flow biocatalysis with recombinant enzymes is that the turn-around time from the idea to the final drug product for the market lead could be significantly

shortened. In the present study, we used the ketoreductase LbADH for stereoselective syntheses as a proof-of-concept. However, our approach should also be applicable for many other enzymes, especially when they are cofactor-dependent, such as P450 monooxygenases [44], imine reductases [45], or transaminases [46]. We therefore anticipate that compartmentalized microfluidic reaction modules equipped with self-immobilizing biocatalysts could be of tremendous utility for a variety of biocatalytic and even chemo-enzymatic cascade reactions.

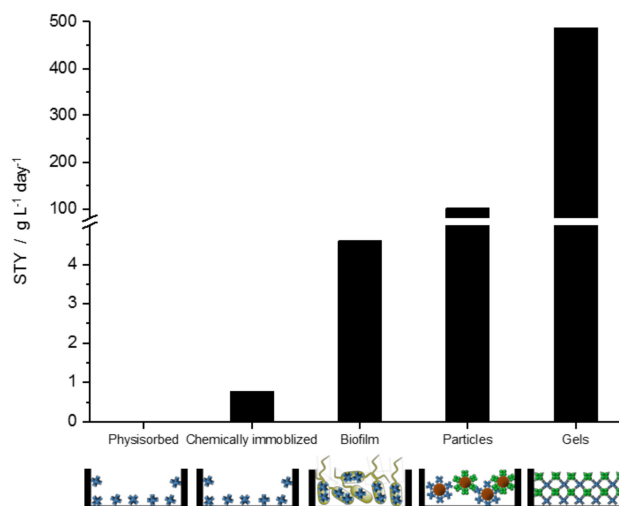


**Figure 4.** Diol **3d** space–time yields (STY) obtained for the various different flow-biocatalysis reactor modules. Schemes of the chip cross section with the immobilized biocatalyst are shown underneath the corresponding bar graphs.

### 3. Materials and Methods

#### 3.1. Cloning of Plasmids

The cloning for all expression plasmids, e.g., for the LbADH and GDH with an SBP-tag [30] or a His-SC/ST-His-tag [23] was previously described.

#### 3.2. Expression, Purification, and Characterization of Enzymes

The expression, purification, and characterization of the proteins was done as described before [23,30]. In brief, *E. coli* BL21(DE3) was transformed with the corresponding expression vector using electroporation. The freshly transformed *E. coli* cells harboring the different plasmids were selected overnight on LB/agar plates containing 100 µg/mL ampicillin at 37 °C. Liquid cultures of 20 mL LB medium containing ampicillin were prepared from the LB/agar plates overnight cultures. The 20 mL cultures were incubated for 14–18 h at 37 °C, 180 rpm in a 150 mL shaking flask and then transferred in 2 L LB-medium containing ampicillin in 4 L shaking flasks and incubated at 37 °C, 180 rpm until the OD<sub>600</sub> reached a value of 0.6. The temperature was then lowered to 25 °C and IPTG was added to a final concentration of 0.1 mM for an additional 16 hours. The cells were harvested by centrifugation (10,000 × g, 10 min) and resuspended in 30 mL buffer A (50 mM NaH<sub>2</sub>PO<sub>4</sub>, 300 mM NaCl, 1 mM MgCl<sub>2</sub>, 10 mM Imidazole, pH 8.0). After disruption by ultrasonication, the cell lysate was obtained by centrifugation (45,000 × g, 1 h), filtered through a 0.45 µm Durapore PVDF membrane (Steriflip, Millipore) and loaded on a HisTrap FF (5 mL) Ni-NTA column (GE Healthcare, Freiburg, Germany) mounted on an Äkta Pure liquid chromatography system (GE Healthcare, Germany). The column was washed with 50 mL buffer A and the 6 × His-tagged proteins were eluted with 100% buffer B (50 mM NaH<sub>2</sub>PO<sub>4</sub>, 300 mM NaCl, 500 mM Imidazole, pH 8.0). For purification of SBP-tagged proteins, a 5 mL Strep-Tactin®Superflow®cartridge (iba-lifescience, Göttingen, Germany) was used according to the manufacturer’s instructions. Subsequently, the

buffer was exchanged for the SBP-tagged GDH and LbADH to 100 mM Triethanolamine pH 7.5, 1 mM MgCl<sub>2</sub> (TEA-Mg), and for GDH-ST and LbADH-SC to 100 mM KP<sub>i</sub> pH 7.5 by Vivaspin 10,000 MWCO (GE Healthcare). The purity of the recombinant, purified proteins was analyzed by standard discontinuous SDS-polyacrylamide Laemmli-midi-gels visualized by Coomassie staining [23,30]. The protein concentrations were determined by UV-Vis spectroscopy, using the theoretical molar extinction coefficients at 280 nm, as calculated by the Geneious version 8.0.5 software [47]. All enzyme activities were in agreement with earlier publications [23,30].

### 3.3. Fabrication of the PDMS Chips

The microfluidic PDMS chips were produced as previously described [40]. In brief, the chip designs were based on the dimension of standard microscope glass slides (76 × 26 mm<sup>2</sup> DIN ISO 8037-1:2003-05). The upper part containing the reaction channel was manufactured by a replica casting of PDMS (Sylgard 184, Dow Corning, Midland, MI, USA) in brass replication molds. Both the meander and linear-shaped channels had a total volume of approximately 150 μL. The meandering channel had a rectangular cross section of 500 × 1000 μm<sup>2</sup>, resulting in a reactor surface of 304 mm<sup>2</sup>, whereas the linear channel used for hydrogel immobilization was 3 mm wide, 1 mm high and 54 mm long, resulting in a reactor surface of 178 mm<sup>2</sup>. Cannulas (Sterican, B. Braun Melsungen AG, Melsungen, Germany), were inserted through horizontal holes in the molds before pouring the PDMS prepolymer to serve as placeholders for the cannulas. The PDMS was cured at 60 °C for at least 3 h. Except for the PDMS chips that were filled with the hydrogel (see 3.7), all PDMS chips were sealed with standard microscope glass slides. To this end, a freshly prepared chip and acetone-cleaned glass slides were plasma-activated in a PlasmaFlecto 10 machine (Plasma technology GmbH, Herrenberg, Germany). Thereafter, the activated surfaces of the PDMS chip and the glass slide were pressed together for covalent binding and subsequently incubated for 15 min at 100 °C.

### 3.4. Preparation and Analysis of Reactor Modules Containing Physisorbed or Chemically Immobilized Enzymes

Chemical immobilization on the meandering PDMS/glass chips was performed following a previously described protocol [48]. For initial cleaning of the chip surface, a piranha solution (seven parts concentrated sulfuric acid, one part 30% hydrogen peroxide solution) was injected into the chip and incubated for 5 min. Thereafter, the channel was washed for 15 min until the pH was neutral with ddH<sub>2</sub>O at a flow rate of 1 mL/min, then for 5 min with 99% EtOH and subsequently for 15 min with ddH<sub>2</sub>O. For the amino-modification the flow channel was filled and incubated with a 10% (3-aminopropyl) triethoxysilan (APTES) solution for 15 min, which was flushed out afterwards with six channel volumes of 100 mM PBS (100 mM KH<sub>2</sub>PO<sub>4</sub>/K<sub>2</sub>HPO<sub>4</sub>, 150 mM NaCl, 1mM MgCl<sub>2</sub>, pH = 7.5) at a flow rate of 500 μL/min. The channel was then filled with a 50% (w/v) aqueous glutaraldehyde solution for 15 min, washed with six channel volumes of PBS and finally incubated with a 10 μM LbADH-SBP in PBS for 15 min.

For the preparation of PDMS/glass chips with physisorbed enzymes, untreated chips were incubated overnight at 4 °C with a 10 μM LbADH-SBP solution. The enzyme-functionalized chips were subsequently washed for 45 min with PBS at a flow rate of 10 μL/min.

To evaluate the catalytic activity, the enzyme functionalized flow chips were placed on the deck of a microfluidic work station and incubated at 30 °C. Syringe pumps with a reaction buffer (10 mM NDK 1, 1 mM NADP<sup>+</sup>, 5% (v/v) 2-propanol in PBS) were connected via polytetrafluorethylen (PTFE) tubing and the reactions were carried out, unless otherwise stated, at 2 μL/min perfusion flowrate. Samples were drawn from the reactor with a previously described autosampler [40] and subsequently analyzed by chiral HPLC as previously described [37].

### 3.5. Preparation and Analysis of Catalytically Active *E. coli* Biofilm Reactor Modules

Experiments with catalytically active biofilms were performed as previously described [40]. In brief, *E. coli* BL21 (DE3) cells were transformed with the plasmid pET\_LbADH-SBP [30] and

cultivated for 24 h at 37 °C in LB medium, containing 100 µg/mL ampicillin, to form a biofilm inside the meandering PDMS/glass chip. The temperature was then reduced to 30 °C and the protein production was induced by an addition of 0.5 mM IPTG to the perfused cultivation medium. After 24 h, the biofilm populated flowcells were perfused with reaction media containing 10 mM NDK 1 at a flowrate of 2 µL/min. Sampling and analysis of the reactor productivity was conducted as described above (see 3.4).

### 3.6. Preparation and Analysis of Microparticle Packed-Bed Modules Containing SBP-Tagged Enzymes

Preparation of the particle reactor was done as previously described [30]. In brief, magnetic Dynabeads M-280 Streptavidin (MB-STV) from Thermo Fisher Scientific were used for immobilization of the SBP-tagged enzymes. The MB-STV were mixed with 1 nmol of the purified SBP-tagged protein/mg MB for 30 min, 30 °C at a tube rotator. The MB-STVs were subsequently washed three times with TEA-Mg and supplemented with 0.01% (v/v) Tween20 (TEA-T-Mg). The enzyme-functionalized MB-STVs were loaded into the individual compartments of a polymethylmethacrylate (PMMA) chip (microfluidic chipshop, Jena, Germany) comprising four linear flow channels that could be connected with each other by PTFE tubing. Filling of the compartments was achieved through a Mini luer-to-pipette adapter and a corresponding loaded pipette tip using a negative flowrate of −50 µL/min. The dimensions of one channel were 58.5 × 1 × 0.2 mm, which corresponded to a reactor volume of 11.7 µL. The magnetic/catalytic zone, which was determined by Nd magnets arranged underneath, had a volume of approximately 10 µL, respectively 7 µL when 4.5 mg beads were loaded (10 mg corresponded to ~6–7 × 10<sup>8</sup> beads with a diameter of 2.7 µm). With an average size of 22.9 µm<sup>2</sup>/particle, the particle loading increased the total reactor surface from approximately 140 mm<sup>2</sup> (empty) to 6700 mm<sup>2</sup>. Filled channels were connected with a short PTFE tubing (internal diameter 0.5 mm) using Mini luer plugs (microfluidic chipshop). The same tubing and plugs were used to connect the inlet of the assembled chip with a CETONI neMESYS base module holding the syringe pump containing the cofactor/substrate solution and the outlet with the CETONI Compact Positioning System rotAXYS, which was controlled by the QmixElements software Qt 5.9.2. (Version: 20180626, CETONI GmbH, Korbussen, Germany). The HT200 temperature-controlled chipholder (ibidi GmbH, Planegg, Germany) was set to hold 30 °C. The chipholder was modified with Nd permanent magnets, positioned beneath the channels of the chip. The syringe pump was filled with a 5 mL cofactor/substrate solution containing 5 mM NDK 1 in TEA-T-Mg, and 1 mM NADP<sup>+</sup> supplemented with 0.01% sodium azide to avoid fouling. For cofactor regeneration, the reaction buffer was either complemented with 5% (v/v) 2-propanol or 100 mM glucose. A flow rate of 1 µL/min was used. The chip outflow was automatically fractionated by the rotAXYS system in a 96-well plate which contained 50 µL 7 M NaClO to stop all enzymatic reactions. The samples were subsequently analyzed by chiral HPLC.

### 3.7. Preparation and Analysis of Hydrogel Reactor Modules

Preparation and analysis of the hydrogel reactor was achieved as previously described [23]. In brief, PDMS chips with a linear channel were placed inside an incubator 1000 (Heidolph, Germany, set to 30 °C), filled with 150 µL protein solution of 1000 µM GDH-ST-His/His-SC-LbADH in KP<sub>i</sub>-Mg (100 mM KP<sub>i</sub> pH 7.5, 1 mM MgCl<sub>2</sub>) and incubated for 30 min. For experiments with gel-entrapped NADP<sup>+</sup>, the protein solution was supplemented with 1 mM NADP<sup>+</sup>. This process was repeated three times and the PDMS chips were then sealed with a glass slide or with a polyolefin foil (HJ-BIOANALYTIK GmbH, Erkelenz, Germany). The NADP<sup>+</sup>-encapsulating hydrogels contained NADP<sup>+</sup> at a final concentration of 10 µM. A pumping unit (Fusion 100, Chemyx Inc., Stafford, TX, USA) with two independent syringe modules equipped with 5 or 20 mL Omnifix syringes (B. Braun Melsungen AG, Melsungen, Germany) was connected to the chip for perfusion of reaction media at a flowrate of 10 µL/min. The syringes were filled with 5–10 mL substrate solution containing 5 mM NDK 1, 100 mM glucose in KP<sub>i</sub>-Mg, supplemented with 0.01% (v/v) sodium azide to avoid fouling,

and 0 or 1 mM NADP<sup>+</sup> depending on the individual experiment. The chip outflow was connected to the Compact Positioning System rotAXYS360 (CETONI GmbH, Korbussen, Germany) to allow for automatic fractioning into 96-well plates. The samples were subsequently analyzed by chiral HPLC.

### 3.8. Chiral HPLC Analysis

Synthesis and the characterization of NDK 1 as well as the analysis of biocatalytic reaction products by chiral HPLC were performed as previously described [37]. In brief, ethyl acetate extractions from the crude reaction mixtures (described above) were dried and resuspended in 100 µL of the mobile phase (90% n-heptane, 10% 2-propanol) and 10–30 µL of the solution was analyzed by HPLC (Agilent 1260 series HPLC equipped with a Diode Array Detector (210 nm) on a Lux 3µ Cellulose-1 (150 × 2.00 mm) chiral column (Phenomenex)). Specific running conditions were used for the analysis of the hydroxy ketones 2 (method A: Chromatography solvent 90% n-heptane/10% 2-propanol, 10 min isocratic, column oven temperature of 10 °C and a flowrate of 0.5 mL/min) and for diol 3 (method B: Chromatography solvent 98% n-heptane/2% 2-propanol, 20 min isocratic, column oven temperature of 45 °C and a flowrate of 1.0 mL/min).

**Author Contributions:** T.P., S.H., J.G., and K.S.R. designed and conceived the characterization of the flow reactors with physisorbed, chemically immobilized enzymes and with the productive biofilm. T.P. and P.B. characterized the enzyme hydrogels under flow conditions. T.P. performed the flow experiments with immobilized particles. T.P., K.S.R., and C.M.N. wrote the manuscript. C.M.N. planned and supervised the project. All authors discussed the results and commented on the manuscript.

**Funding:** This research was funded by the Helmholtz programme, “BioInterfaces in Technology and Medicine” and DFG project Ni399/15-1. PB is grateful for a Kekulé fellowship by Fonds der Chemischen Industrie.

**Acknowledgments:** We thank Sabrina Gallus for the support with the hydrogel development.

**Conflicts of Interest:** The authors declare no conflict of interest.

## References

1. Straathof, A.J. Transformation of biomass into commodity chemicals using enzymes or cells. *Chem. Rev.* **2014**, *114*, 1871–1908. [[CrossRef](#)] [[PubMed](#)]
2. Sheldon, R.A.; Woodley, J.M. Role of Biocatalysis in Sustainable Chemistry. *Chem. Rev.* **2017**, *118*, 801–838. [[CrossRef](#)] [[PubMed](#)]
3. Liang, J.; Lalonde, J.; Borup, B.; Mitchell, V.; Mundorff, E.; Trinh, N.; Kochrekar, D.A.; Cherat, R.N.; Pai, G.G. Development of a Biocatalytic Process as an Alternative to the (–)-DIP-Cl-Mediated Asymmetric Reduction of a Key Intermediate of Montelukast. *Org. Process Res. Dev.* **2010**, *14*, 193–198. [[CrossRef](#)]
4. Ma, S.K.; Gruber, J.; Davis, C.; Newman, L.; Gray, D.; Wang, A.; Grate, J.; Huisman, G.W.; Sheldon, R.A. A green-by-design biocatalytic process for atorvastatin intermediate. *Green Chem.* **2010**, *12*, 81–86. [[CrossRef](#)]
5. Han, C.; Savage, S.; Al-Sayah, M.; Yajima, H.; Remarchuk, T.; Reents, R.; Wirz, B.; Iding, H.; Bachmann, S.; Fantasia, S.M.; et al. Asymmetric Synthesis of Akt Kinase Inhibitor Ipatasertib. *Org. Lett.* **2017**, *19*, 4806–4809. [[CrossRef](#)] [[PubMed](#)]
6. Savile, C.K.; Janey, J.M.; Mundorff, E.C.; Moore, J.C.; Tam, S.; Jarvis, W.R.; Colbeck, J.C.; Krebber, A.; Fleitz, F.J.; Brands, J. Biocatalytic Asymmetric Synthesis of Chiral Amines from Ketones Applied to Sitagliptin Manufacture. *Science* **2010**, *329*, 305–309. [[CrossRef](#)] [[PubMed](#)]
7. Chen, A.H.; Silver, P.A. Designing biological compartmentalization. *Trends Cell Biol.* **2012**, *22*, 662–670. [[CrossRef](#)]
8. Wheeldon, I.; Minter, S.D.; Banta, S.; Barton, S.C.; Atanassov, P.; Sigman, M. Substrate channelling as an approach to cascade reactions. *Nat. Chem.* **2016**, *8*, 299–309.
9. Kuchler, A.; Yoshimoto, M.; Luginbuhl, S.; Mavelli, F.; Walde, P. Enzymatic reactions in confined environments. *Nat. Nanotechnol.* **2016**, *11*, 409–420.
10. Chen, Z.; Zeng, A.P. Protein engineering approaches to chemical biotechnology. *Curr. Opin. Biotechnol.* **2016**, *42*, 198–205.
11. Quin, M.B.; Wallin, K.K.; Zhang, G.; Schmidt-Dannert, C. Spatial organization of multi-enzyme biocatalytic cascades. *Org. Biomol. Chem.* **2017**. [[CrossRef](#)] [[PubMed](#)]

12. France, S.P.; Hepworth, L.J.; Turner, N.J.; Flitsch, S.L. Constructing Biocatalytic Cascades: In Vitro and in Vivo Approaches to de Novo Multi-Enzyme Pathways. *ACS Catal.* **2017**, *7*, 710–724. [[CrossRef](#)]
13. Rabe, K.S.; Muller, J.; Skoupi, M.; Niemeyer, C.M. Cascades in Compartments: En Route to Machine-Assisted Biotechnology. *Angew. Chem. Int. Ed.* **2017**, *56*, 13574–13589. [[CrossRef](#)]
14. Ley, S.V.; Fitzpatrick, D.E.; Ingham, R.J.; Myers, R.M. Organic synthesis: march of the machines. *Angew. Chem. Int. Ed.* **2015**, *54*, 3449–3464. [[CrossRef](#)] [[PubMed](#)]
15. Li, J.; Ballmer, S.G.; Gillis, E.P.; Fujii, S.; Schmidt, M.J.; Palazzolo, A.M.; Lehmann, J.W.; Morehouse, G.F.; Burke, M.D. Synthesis of many different types of organic small molecules using one automated process. *Science* **2015**, *347*, 1221–1226. [[CrossRef](#)]
16. Adamo, A.; Beingessner, R.L.; Behnam, M.; Chen, J.; Jamison, T.F.; Jensen, K.F.; Monbaliu, J.C.; Myerson, A.S.; Revalor, E.M.; Snead, D.R. On-demand continuous-flow production of pharmaceuticals in a compact, reconfigurable system. *Science* **2016**, *352*, 61–67. [[CrossRef](#)] [[PubMed](#)]
17. Plutschack, M.B.; Pieber, B.; Gilmore, K.; Seeberger, P.H. The Hitchhiker’s Guide to Flow Chemistry(II). *Chem. Rev.* **2017**, *117*, 11796–11893. [[CrossRef](#)]
18. Matosevic, S.; Szita, N.; Baganz, F. Fundamentals and applications of immobilized microfluidic enzymatic reactors. *J. Chem. Technol. Biotechnol.* **2011**, *86*, 325–334. [[CrossRef](#)]
19. Wohlgemuth, R.; Plazl, I.; Znidarsic-Plazl, P.; Gernaey, K.V.; Woodley, J.M. Microscale technology and biocatalytic processes: opportunities and challenges for synthesis. *Trends Biotechnol.* **2015**, *33*, 302–314. [[CrossRef](#)]
20. Tamborini, L.; Fernandes, P.; Paradisi, F.; Molinari, F. Flow Bioreactors as Complementary Tools for Biocatalytic Process Intensification. *Trends Biotechnol.* **2017**. [[CrossRef](#)]
21. Britton, J.; Majumdar, S.; Weiss, G.A. Continuous flow biocatalysis. *Chem. Soc. Rev.* **2018**. [[CrossRef](#)] [[PubMed](#)]
22. Maier, M.; Radtke, C.P.; Hubbuch, J.; Niemeyer, C.M.; Rabe, K.S. On-Demand Production of Flow-Reactor Cartridges by 3D Printing of Thermostable Enzymes. *Angew. Chem. Int. Ed.* **2018**, *57*, 5539–5543. [[CrossRef](#)] [[PubMed](#)]
23. Peschke, T.; Bitterwolf, P.; Gallus, S.; Hu, Y.; Oelschlaeger, C.; Willenbacher, N.; Rabe, K.S.; Niemeyer, C.M. Self-Assembling All-Enzyme Hydrogels for Flow Biocatalysis. *Angew. Chem. Int. Ed.* **2018**, *57*, 17028–17032. [[CrossRef](#)] [[PubMed](#)]
24. Thompson, M.P.; Peñafiel, I.; Cosgrove, S.C.; Turner, N.J. Biocatalysis Using Immobilized Enzymes in Continuous Flow for the Synthesis of Fine Chemicals. *Org. Process Res. Dev.* **2018**. [[CrossRef](#)]
25. Schmid-Dannert, C.; Lopez-Gallego, F. Advances and opportunities for the design of self-sufficient and spatially organized cell-free biocatalytic systems. *Curr. Opin. Chem. Biol.* **2018**, *49*, 97–104. [[CrossRef](#)] [[PubMed](#)]
26. Gandomkar, S.; Żądło-Dobrowolska, A.; Kroutil, W. Extending Designed Linear Biocatalytic Cascades for Organic Synthesis. *ChemCatChem* **2019**, *11*, 225–243. [[CrossRef](#)]
27. Buchholz, K.; Kasche, V.; Bornscheuer, U.T. *Biocatalysts and Enzyme Technology-2nd Edition*; Wiley-Blackwell: Weinheim, Germany, 2012; 444p.
28. Jonkheijm, P.; Weinrich, D.; Schroeder, H.; Niemeyer, C.M.; Waldmann, H. Chemical Strategies for Generating Protein Biochips. *Angew. Chem. Int. Ed.* **2008**, *47*, 9618–9647. [[CrossRef](#)]
29. Britton, J.; Dyer, R.P.; Majumdar, S.; Raston, C.L.; Weiss, G.A. Ten-Minute Protein Purification and Surface Tethering for Continuous-Flow Biocatalysis. *Angew. Chem. Int. Ed.* **2017**, *56*, 2296–2301. [[CrossRef](#)]
30. Peschke, T.; Skoupi, M.; Burgahn, T.; Gallus, S.; Ahmed, I.; Rabe, K.S.; Niemeyer, C.M. Self-Immobilizing Fusion Enzymes for Compartmentalized Biocatalysis. *ACS Catal.* **2017**, *7*, 7866–7872. [[CrossRef](#)]
31. Contente, M.L.; Paradisi, F. Self-sustaining closed-loop multienzyme-mediated conversion of amines into alcohols in continuous reactions. *Nat. Catal.* **2018**, *1*, 452–459. [[CrossRef](#)]
32. Mohamad, N.R.; Marzuki, N.H.; Buang, N.A.; Huyop, F.; Wahab, R.A. An overview of technologies for immobilization of enzymes and surface analysis techniques for immobilized enzymes. *Biotechnol. Biotechnol. Equip.* **2015**, *29*, 205–220. [[CrossRef](#)] [[PubMed](#)]
33. Misson, M.; Zhang, H.; Jin, B. Nanobiocatalyst advancements and bioprocessing applications. *J. R. Soc. Interface* **2015**, *12*, 20140891. [[CrossRef](#)]
34. Gkantzou, E.; Patila, M.; Stamatis, H. Magnetic Microreactors with Immobilized Enzymes-From Assemblage to Contemporary Applications. *Catalysts* **2018**, *8*, 282. [[CrossRef](#)]

35. Qureshi, N.; Annous, B.A.; Ezeji, T.C.; Karcher, P.; Maddox, I.S. Biofilm reactors for industrial bioconversion processes: employing potential of enhanced reaction rates. *Microb. Cell Fact.* **2005**, *4*, 24. [[CrossRef](#)] [[PubMed](#)]
36. Leuchs, S.; Greiner, L. Alcohol Dehydrogenase from *Lactobacillus brevis*: A Versatile Robust Catalyst for Enantioselective Transformations. *Chem. Biochem. Engin. Q.* **2011**, *25*, 267–281.
37. Skoupi, M.; Vaxelaire, C.; Strohmman, C.; Christmann, M.; Niemeyer, C.M. Enantiogroup-Differentiating Biocatalytic Reductions of Prochiral Cs-Symmetrical Dicarboxyl Compounds to meso Compounds. *Chem. Eur. J.* **2015**, *21*, 8701–8705. [[CrossRef](#)]
38. Keefe, A.D.; Wilson, D.S.; Seelig, B.; Szostak, J.W. One-step purification of recombinant proteins using a nanomolar-affinity streptavidin-binding peptide, the SBP-Tag. *Protein Expr. Purif.* **2001**, *23*, 440–446. [[CrossRef](#)]
39. Zhao, X.; Li, G.; Liang, S. Several affinity tags commonly used in chromatographic purification. *J. Anal. Methods Chem.* **2013**, *2013*, 581093. [[CrossRef](#)]
40. Hansen, S.H.; Kabbeck, T.; Radtke, C.P.; Krause, S.; Krolitzki, E.; Peschke, T.; Gasmi, J.; Rabe, K.S.; Wagner, M.; Horn, H.; et al. Machine-assisted cultivation and analysis of biofilms. *bioRxiv* **2017**. [[CrossRef](#)]
41. Peschke, T.; Rabe, K.S.; Niemeyer, C.M. Orthogonal Surface Tags for Whole-Cell Biocatalysis. *Angew. Chem. Int. Ed.* **2017**, *56*, 2183–2186. [[CrossRef](#)]
42. Zakeri, B.; Fierer, J.O.; Celik, E.; Chittock, E.C.; Schwarz-Linek, U.; Moy, V.T.; Howarth, M. Peptide tag forming a rapid covalent bond to a protein, through engineering a bacterial adhesin. *Proc. Natl. Acad. Sci. USA* **2012**, *109*, E690–697. [[CrossRef](#)] [[PubMed](#)]
43. Liu, W.; Wang, P. Cofactor regeneration for sustainable enzymatic biosynthesis. *Biotechnol. Adv.* **2007**, *25*, 369–384. [[CrossRef](#)] [[PubMed](#)]
44. Urlacher, V.B.; Girhard, M. Cytochrome P450 monooxygenases: an update on perspectives for synthetic application. *Trends Biotechnol.* **2012**, *30*, 26–36. [[CrossRef](#)] [[PubMed](#)]
45. Mangas-Sanchez, J.; France, S.P.; Montgomery, S.L.; Aleku, G.A.; Man, H.; Sharma, M.; Ramsden, J.I.; Grogan, G.; Turner, N.J. Imine reductases (IREDs). *Curr. Opin. Chem. Biol.* **2017**, *37*, 19–25. [[CrossRef](#)] [[PubMed](#)]
46. Guo, F.; Berglund, P. Transaminase biocatalysis: optimization and application. *Green Chem.* **2017**, *19*, 333–360. [[CrossRef](#)]
47. Kearse, M.; Moir, R.; Wilson, A.; Stones-Havas, S.; Cheung, M.; Sturrock, S.; Buxton, S.; Cooper, A.; Markowitz, S.; Duran, C. Geneious Basic: an integrated and extendable desktop software platform for the organization and analysis of sequence data. *Bioinformatics* **2012**, *28*, 1647–1649. [[CrossRef](#)] [[PubMed](#)]
48. Thomsen, M.S.; Nidetzky, B. Microfluidic reactor for continuous flow biotransformations with immobilized enzymes: The example of lactose hydrolysis by a hyperthermophilic beta-glycoside hydrolase. *Eng. Life Sci.* **2008**, *8*, 40–48. [[CrossRef](#)]

